

# Effect of substitutional doping on the Néel temperature of $\text{Cr}_2\text{O}_3$

Sai Mu, A. L. Wysocki, and K. D. Belashchenko\*

*Department of Physics and Astronomy, Nebraska Center for Materials and Nanoscience, University of Nebraska-Lincoln, Lincoln, Nebraska 68588, USA*

(Received 13 July 2012; revised manuscript received 26 November 2012; published 28 February 2013)

First-principles calculations are used to explore the possibility of enhancing the Néel temperature  $T_N$  of the magnetoelectric antiferromagnet  $\text{Cr}_2\text{O}_3$  by substitutional doping. We describe the electronic structure of transition metal (V, Ti, Mn, Fe, Co, and Ni) and anion (N and B) impurities and evaluate their effect on the exchange interaction. We find that, although transition-metal impurities and N are likely to reduce  $T_N$ , substitution of O by B is likely to increase it. Both N and B impurities introduce impurity states mediating strong hybridization and magnetic interaction between the neighboring Cr ions. For N impurities, this leads to magnetic frustration, but in the case of B substitution, the stability of the ground antiferromagnetic state is enhanced.

DOI: [10.1103/PhysRevB.87.054435](https://doi.org/10.1103/PhysRevB.87.054435)

PACS number(s): 75.50.Ee, 71.55.-i, 75.85.+t

## I. INTRODUCTION

Magnetoelectric antiferromagnets<sup>1</sup> have attracted considerable attention due to their possible applications in magnetoelectronic devices utilizing electric control of magnetization.<sup>2–5</sup> These materials provide a functional alternative to multiferroics<sup>6–9</sup> for such applications as nonvolatile magnetoelectric memory.<sup>4,10</sup>

$\text{Cr}_2\text{O}_3$  has the highest Néel temperature ( $T_N = 307$  K) among the well-characterized magnetoelectric antiferromagnets, which allows for room-temperature operation<sup>5</sup> in temperature-controlled conditions but does not provide enough flexibility for practical applications. It is, therefore, desirable to find a way to achieve higher  $T_N$  by suitable alloying. Indeed, the magnetic interaction in  $\text{Cr}_2\text{O}_3$  appears to be controlled by direct Cr-Cr exchange,<sup>11</sup> which is sensitive to the interatomic distances and can, therefore, be manipulated by atomic relaxations induced by dopants. Furthermore, impurity states introduced by a dopant can also provide additional exchange coupling between the Cr atoms of the host; this situation is familiar from the studies of diluted magnetic semiconductors.<sup>12</sup> On the other hand, in order to be usable as a switchable magnetoelectric device, the doped material should remain a good insulator. Therefore, the impurity states introduced by the dopant should not result in a narrow excitation gap.

In this paper, we investigate a number of potential substitutional dopants, both on the cation and on the anion sites in  $\text{Cr}_2\text{O}_3$  using electronic structure calculations based on the local-density approximation (LDA) +  $U$  method.<sup>13</sup> This method provides a very good description of the structural, electronic, and magnetic properties of bulk  $\text{Cr}_2\text{O}_3$ ,<sup>11</sup> and it has been used to characterize transition-metal impurities in hematite.<sup>14</sup> In order to assess the effect of the dopant on the Néel temperature, we calculate the effective exchange field experienced by the transition-metal dopant as well as by the nearby Cr atoms (for both transition-metal and anion dopants) as the energy difference between the ground state (GS) and the state in which the local moment of the corresponding atom is reversed.

Based on our results, we propose B as a promising dopant and predict that it should increase  $T_N$  of  $\text{Cr}_2\text{O}_3$  by approximately 10% per 1% of O site substitution by B. For the

favorable midgap position of the Fermi level, the B impurity is expected to be in a neutral charged state with an excitation gap of about 2 eV.

## II. COMPUTATIONAL METHODS

The impurities were introduced using two kinds of supercells. The first kind is the conventional hexagonal unit cell, which is often used for bulk  $\text{Cr}_2\text{O}_3$ . The second, “mixed” kind of cell was also considered in order to increase the in-plane separation between the impurities. This mixed cell was constructed by enlarging the in-plane hexagonal lattice vectors by  $\sqrt{3}$  and taking one of the rhombohedral translations as the third translation vector. The two cell kinds are shown in Fig. 1; both contain 30 atoms. Comparison of the results obtained with different supercells allows us to estimate the degree to which the finite size of the cell affects the electronic and magnetic properties. In all calculations, one Cr or O atom in the cell was replaced by an impurity atom. The ionic coordinates were relaxed while keeping the cell shape and volume fixed at their equilibrium values for bulk  $\text{Cr}_2\text{O}_3$ .

The details of the electronic structure calculations were similar to those of Ref. 11, including the use of the rotationally invariant LDA +  $U$  method<sup>13</sup> with  $U = 4$  and  $J = 0.58$  eV. (The same values of  $U$  and  $J$  were employed for all transition-metal impurities.) The Kohn-Sham equations were solved using the projector augmented-wave method<sup>15</sup> as implemented in the Vienna *ab initio* simulation package code.<sup>16,17</sup> We used the plane-wave energy cutoff of 520 eV and  $\Gamma$ -centered Monkhorst-Pack grids<sup>18</sup> for the Brillouin zone integration. Gaussian smearing of 0.1 eV (0.02 eV) and a  $4 \times 4 \times 2$  ( $8 \times 8 \times 4$ )  $k$ -point mesh were used for ionic relaxation [density of states (DOS) calculation] for the hexagonal cell. Similar parameters were employed for the mixed cell, except that the  $k$ -point mesh was  $3 \times 3 \times 5$ . The Hellmann-Feynman forces were converged to 0.005 eV/Å.

In order to assess the effect of an impurity on the Néel temperature of  $\text{Cr}_2\text{O}_3$ , we evaluated the exchange energies for the Cr neighbors of the impurity as well as for the cation impurities themselves. The exchange energy for the given ion is defined as the energy separation between the magnetic ground state and the state in which the local moment on the

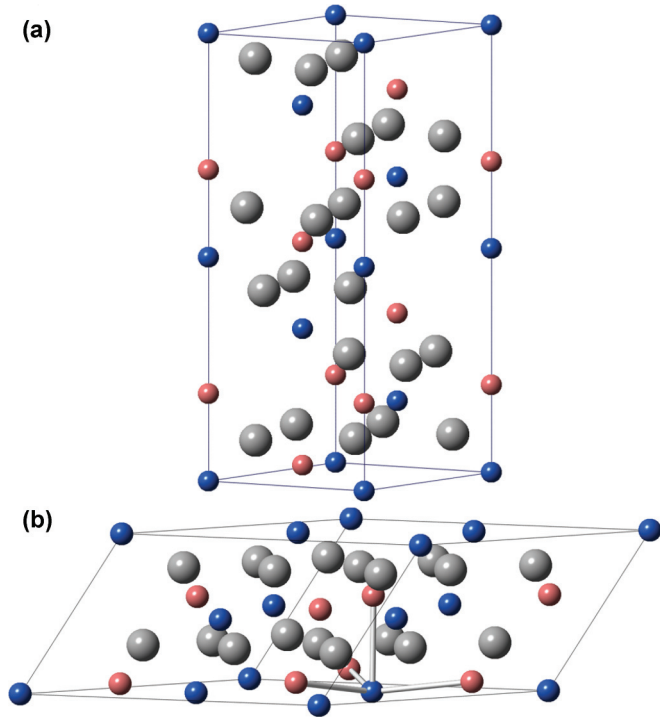


FIG. 1. (Color online) (a) Hexagonal supercell. (b) Mixed supercell. Smaller blue (darker) and red (lighter) spheres: Cr atoms with different directions of the local moment. Larger gray spheres: O atoms. Bars show the nearest Cr neighbor along the  $c$  axis and three next-nearest Cr neighbors for one Cr atom.

given ion is reversed. (In the Heisenberg model, the exchange energy  $E_i$  on site  $i$  is given by  $E_i = 2 \sum_j J_{ij}$ , where  $J_{ij}$  is the Heisenberg model parameter; the local moments and their signs are here absorbed in the definition of the exchange energy.) For the homogeneous system with equivalent sites, the mean-field  $T_N$  for the quantum spin- $S$  Heisenberg model is equal to  $1/6$  of the exchange energy multiplied by  $(S + 1)/S$ . The difference in the exchange energies at the impurity and at the nearby Cr atoms from Cr in the bulk can be used to evaluate the effect of that impurity on  $T_N$ . We do not attempt to calculate the modification of  $T_N$  accurately, restricting ourselves to qualitative estimates.

### III. BULK $\text{Cr}_2\text{O}_3$

$\text{Cr}_2\text{O}_3$  crystallizes in the corundum structure (space group  $R\bar{3}c$ ). It can be viewed as a stacking of buckled honeycomb Cr double layers along the (0001) direction with quasi-hexagonal close-packed O layers in between (see Fig. 1). Crystallographically, all Cr ions are equivalent. Each Cr has one nearest-neighbor Cr atom along the (0001) direction and three next-nearest-neighbor Cr atoms within the same honeycomb layer. Since the crystal field on the Cr site is approximately octahedral, it is customary to classify the Cr  $3d$  electronic states into  $t_{2g}$  and  $e_g$  sub-bands. Throughout this paper, the terms  $t_{2g}$  and  $e_g$  are used in this approximate sense. However, the actual local symmetry at the Cr site is  $C_3$ , and consequently, the  $t_{2g}$  states are slightly split into a lower-lying doublet and

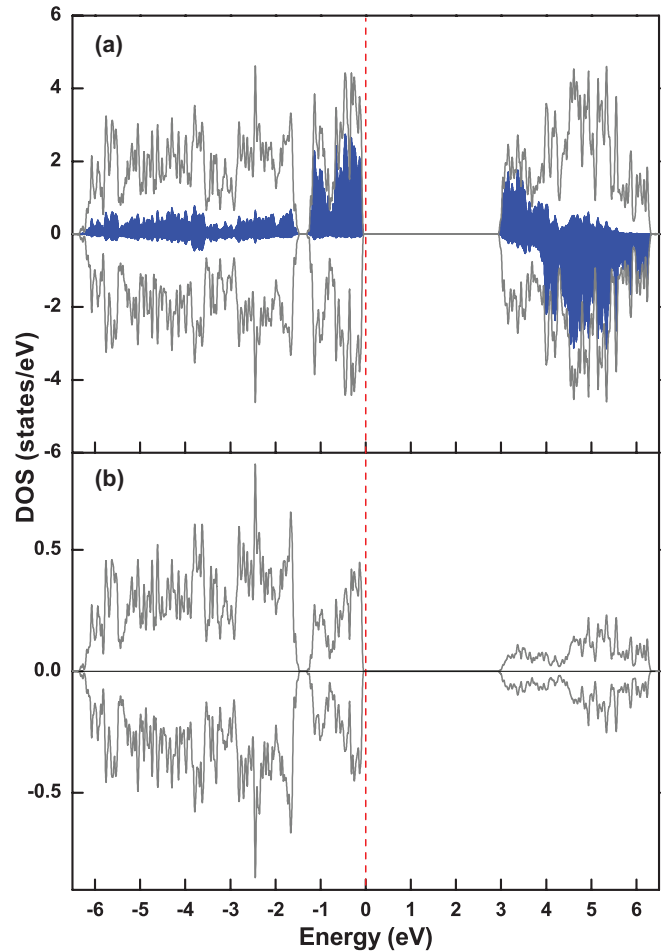


FIG. 2. (Color online) Total and partial DOS for bulk  $\text{Cr}_2\text{O}_3$ . (a) Total DOS per formula unit (solid line) and partial Cr  $3d$  DOS per Cr site (blue shaded area). (b) Partial O  $2p$  DOS per O site. Majority- and minority-spin DOS are plotted as positive and negative, respectively. The dashed vertical line indicates the valence-band maximum.

a higher-lying singlet. The  $e_g$  states hybridize strongly with O  $2p$  states.

The electronic structure of  $\text{Cr}_2\text{O}_3$  was studied by several authors;<sup>11,19,20</sup> our calculation details here are the same as in Ref. 11. For further reference, the total and partial DOS of  $\text{Cr}_2\text{O}_3$  are shown in Fig. 2. The occupied Cr states are almost fully spin polarized. The top of the valence band is formed by majority-spin Cr  $t_{2g}$  states separated by a small gap from the O  $2p$  states; the latter are strongly hybridized with Cr  $e_g$ . The calculated fundamental band gap is 3.0 eV, which is close to the experimental 3.4 eV. At the bottom of the conduction band, there are majority-spin Cr  $e_g$  states. The minority-spin Cr  $3d$  states (both  $t_{2g}$  and  $e_g$ ) lie somewhat higher.

The local magnetic moment on Cr is  $2.86\mu_B$ , which is close to the ionic limit of  $3\mu_B$ . The antiferromagnetic order is shown in Fig. 1. Magnetism can be well described by the Heisenberg Hamiltonian with strong exchange interactions with the first two shells of neighbors and additional weak interactions up to the fifth-neighbor shell.<sup>11,21</sup> The exchange interaction in  $\text{Cr}_2\text{O}_3$  is, to a large extent, controlled by direct-hopping Cr-Cr exchange, whereas, superexchange through O is ineffective.<sup>11</sup>

TABLE I. Distances from the dopant ions to its nearest ( $d_1$ ) and next-nearest ( $d_2$ ) Cr neighbors and to its O neighbors in the nearest ( $d_3$ ) and next-nearest ( $d_4$ ) O layer (all in Å) as well as the local magnetic moment  $m_d$  ( $\mu_B$ ) of the dopant ion (the local moment in the ionic picture is given in brackets). Different values of the three second-neighbor distances indicate the presence of a Jahn-Teller distortion. The corresponding values are given for both hexagonal and mixed cells. The impurities are isovalent unless the formal ionic charge is specified.

Dopant	Ti		Ti <sup>4+</sup>		V		Cr	Mn		Fe		Co		Ni		Ni <sup>2+</sup>				
	Hex	Mix	Hex	Mix	Hex	Mix	Bulk	Hex	Mix	Hex	Mix	Hex	Mix	Hex	Mix	Hex	Mix			
$d_1$	2.72	2.70	2.73	2.72	2.70	2.69	2.65	2.67	(2.68)	2.67	2.70	2.71	2.59	2.61	2.62	2.63	2.63	2.67		
$d_2$	2.85	2.88		2.91				2.87	(2.88)	2.88					2.87	2.87				
	2.90	2.91	2.89	2.92	2.89	2.89	2.88	2.89	(2.89)	2.88	2.90	2.89	2.88	2.86	2.88	2.87	2.89	2.87		
	2.92	2.93		2.93				2.90	(2.90)	2.89					2.90	2.87				
$d_3$	1.96	1.96		1.92				1.92	(1.90)	1.91					1.89	(1.88)	1.89			
	2.02	2.01	1.93	1.93	1.97	1.97	1.96	1.93	(1.99)	1.94	1.94	1.93	1.91	1.92	1.91	(1.95)	1.95	1.97	1.97	
	2.02	2.02		1.93				2.03	(1.99)	2.02					1.99	(1.96)	1.97			
$d_4$	2.05	2.05		2.03				1.98	(1.95)	1.98					1.93	(1.91)	1.92			
	2.09	2.09	2.02	2.03	2.04	2.04	2.01	1.99	(2.08)	2.01	2.06	2.07	1.93	1.93	1.95	(2.01)	2.00	2.02	2.06	
	2.10	2.10		2.04				2.14	(2.09)	2.13					2.05	(2.02)	2.02			
$m_d$	0.88	(1)	-0.01	(0)	1.87	(2)	2.86	(3)	3.72	(4)	4.14	(5)	0.03	(0)	-0.04	(0)	0.88	(1)	1.59	(2)

#### IV. TRANSITION-METAL IMPURITIES

In this section, we discuss the transition-metal impurities in Cr<sub>2</sub>O<sub>3</sub>. In most cases, we assume isovalent substitution, but the natural Ti<sup>4+</sup> and Ni<sup>2+</sup> charge states are also considered. First, we describe the formation of the impurity levels and their occupation and then proceed to structural features and exchange energies. The DOS for different dopants in the hexagonal supercell are shown in Figs. 3–8; those for the mixed supercell are quite similar (see Supplemental Material<sup>22</sup>). Table I lists the distances from the dopant atoms to their Cr and O neighbors as well as the values of the local magnetic moment on the impurity atom. (Although the mixed supercell breaks the C<sub>3</sub> symmetry of the Cr sites, the resulting differences in the bond lengths are in the milliangstrom range and are not seen in the table.) Furthermore, exchange energies for the dopants and for the nearby Cr atoms are given in Table II.

##### A. Impurity levels

In the ionic picture, the Ti<sup>3+</sup> ion has one 3*d* electron, which occupies a majority-spin impurity level (see Fig. 3). Since the charge of the Ti nucleus is smaller than that of Cr, the electronic states of Ti lie higher in energy compared

to those of Cr; this results in a deep approximately midgap impurity level. The impurity state is *t*<sub>2*g*</sub>-like and is split off from the unoccupied Ti *t*<sub>2*g*</sub> majority states by the Hubbard *U* interaction. The unoccupied Ti states lie inside the conduction band.

The V<sup>3+</sup> ion is formally 3*d*<sup>2</sup>, and a doubly occupied *t*<sub>2*g*</sub>-like impurity level is seen in the majority-spin partial DOS (Fig. 4). As for the Ti dopant, the occupied impurity states fall into the band gap. However, these states are much shallower compared to the case of Ti. The remaining majority-spin V *t*<sub>2*g*</sub> state is empty and lies in the band gap close to the conduction-band minimum. This state is split off from the occupied majority-spin V *t*<sub>2*g*</sub> states by the Hubbard *U* interaction. On the other hand, the majority-spin V *e*<sub>g</sub> and all minority-spin V 3*d* states lie in the conduction band.

The partial DOS for the Mn ion is shown in Fig. 5. The Mn<sup>3+</sup> ion is formally 3*d*<sup>4</sup>. Its filled majority-spin *t*<sub>2*g*</sub> states lie deeper compared to those of Cr and hybridize strongly with the valence-band states. The remaining one valence electron occupies one of the majority-spin *e*<sub>g</sub>-like levels, forming a deep impurity state in the band gap. This state is separated by about 1 eV from the empty Mn majority-spin *e*<sub>g</sub> state, which is mainly the effect of the Hubbard *U* interaction. As for the other

TABLE II. Exchange energies (meV units) for transition-metal dopants ( $E_0$ ) and for their nearest ( $E_1$ ) and next-nearest ( $E_2$ ) Cr neighbors in the hexagonal and mixed supercells.

	Hexagonal cell									
	Ti	Ti <sup>4+</sup>	V	Cr	Mn	Fe	Co	Ni	Ni <sup>2+</sup>	
$E_0$	112		75	120	90	90		11		-13
$E_1$	97	92	84		107	131	90	97		110
$E_2$	123	40	120		92	117	83	122		72
	Mixed cell									
	Ti	Ti <sup>4+</sup>	V	Cr	Mn	Fe	Co	Ni	Ni <sup>2+</sup>	
$E_0$	108		74	121	89	92		-10		-5
$E_1$	87	99	72		102	166	122	138		128
$E_2$	186, 97, 104	93, 95, 86	120		122, 105, 108	124	103	69, 94, 103		94

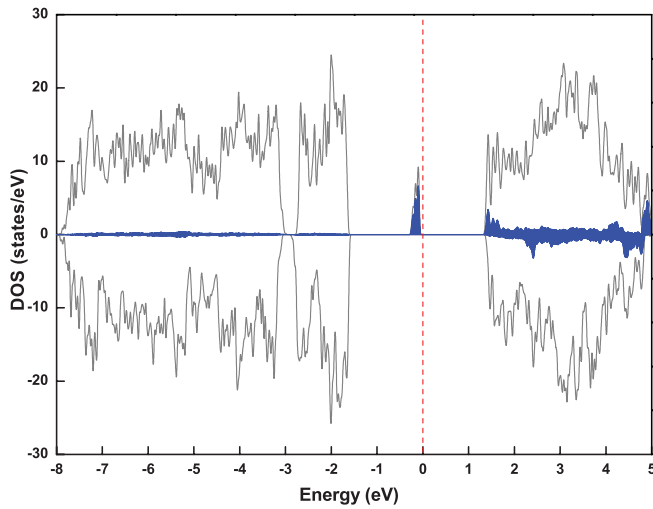


FIG. 3. (Color online) DOS for the  $\text{Ti}^{3+}$  impurity in  $\text{Cr}_2\text{O}_3$ . The unfilled black line is the total DOS, whereas, the blue shaded area indicates the local DOS on the Ti impurity. Majority- and minority-spin DOS are plotted as positive and negative, respectively. The dashed vertical line indicates the energy of the highest filled state. Similar conventions are used in all subsequent figures.

dopants considered above, the exchange interaction shifts the minority-spin Mn  $3d$  states into the conduction band.

The  $\text{Fe}^{3+}$  ion has a half-filled  $3d$  shell (configuration  $3d^5$ ). As seen in the partial DOS (see Fig. 6), these five electrons fully occupy the majority-spin Fe  $3d$  states. The large nuclear charge of Fe pulls these states below the Cr  $3d$  levels. The majority-spin Fe  $e_g$  states strongly hybridize with the O  $2p$  states. The majority-spin Fe  $t_{2g}$  states do not strongly overlap with O  $2p$  states and form a rather narrow impurity band about 6.5 eV below the valence-band maximum. The empty minority-spin Fe  $3d$  states fall below the minority-spin Cr  $3d$  states and end up in the band gap. These minority-spin impurity states are split by the crystal field into deep  $t_{2g}$  impurity levels and shallow  $e_g$  states near the conduction-band minimum.

Due to the fully filled majority-spin Fe  $d$  shell, the local moment on Fe ( $4.14\mu_B$ ) is the largest in the series (see Table I).

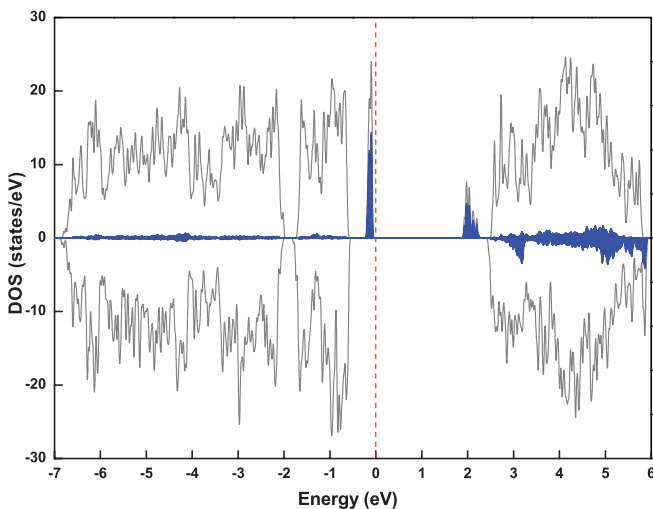


FIG. 4. (Color online) DOS for the  $\text{V}^{3+}$  impurity in  $\text{Cr}_2\text{O}_3$ .

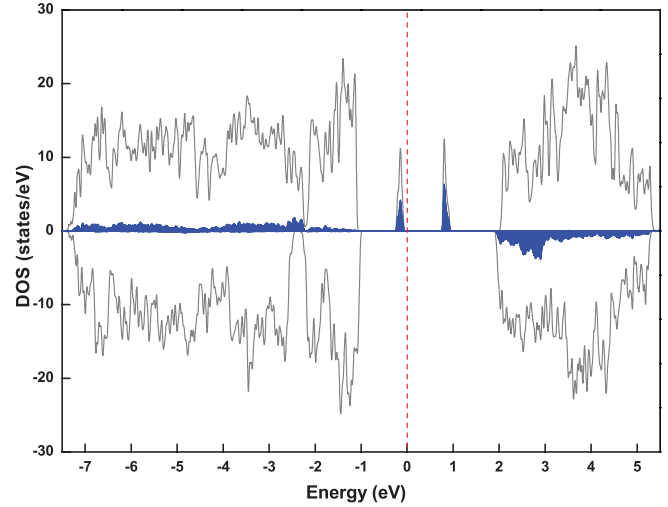


FIG. 5. (Color online) DOS for the  $\text{Mn}^{3+}$  impurity in  $\text{Cr}_2\text{O}_3$ .

However, it is significantly reduced compared to the ideal value of  $5\mu_B$  due to strong hybridization between the Fe  $e_g$  levels and the O  $2p$  states.

The  $\text{Co}^{3+}$  ion adds one electron (configuration  $3d^6$ ). Depending on the relation among the crystal field, Hubbard  $U$  interaction, and exchange splitting, this ion can be found in different spin states. Starting from different charge densities in the self-consistent procedure, we were able to converge the high-spin ( $3d^5_↑3d^1_↓$ ) and the low-spin ( $3d^3_↑3d^3_↓$ ) states. Such behavior is common for the LDA +  $U$  method since the Hubbard term produces local minima in the energy functional for configurations with occupancies close to integer values.<sup>23</sup> The true ground state is the solution with the lowest energy, which, for Co, is the low-spin state with a nearly zero local moment. The partial DOS for Co in this low-spin state is shown in Fig. 7. The  $t_{2g}$  states of both spin directions are occupied and lie in the region of the majority-spin Cr  $t_{2g}$  states. On the other hand, the empty Co  $e_g$ -like states form impurity levels in the band gap, which lie fairly close to the conduction band.

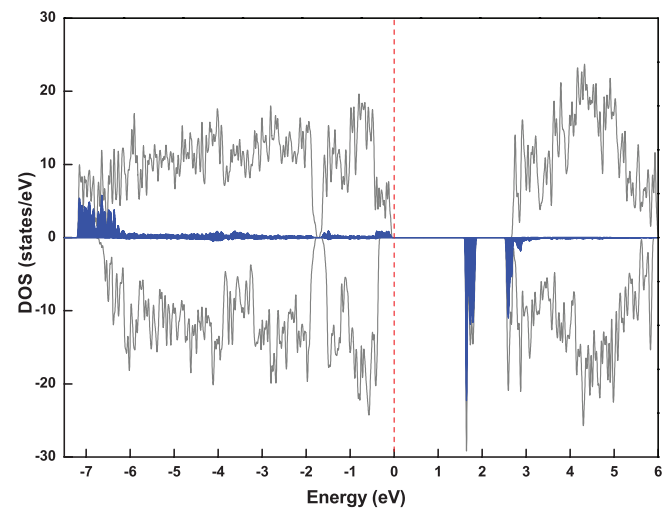


FIG. 6. (Color online) DOS for the  $\text{Fe}^{3+}$  impurity in  $\text{Cr}_2\text{O}_3$ .

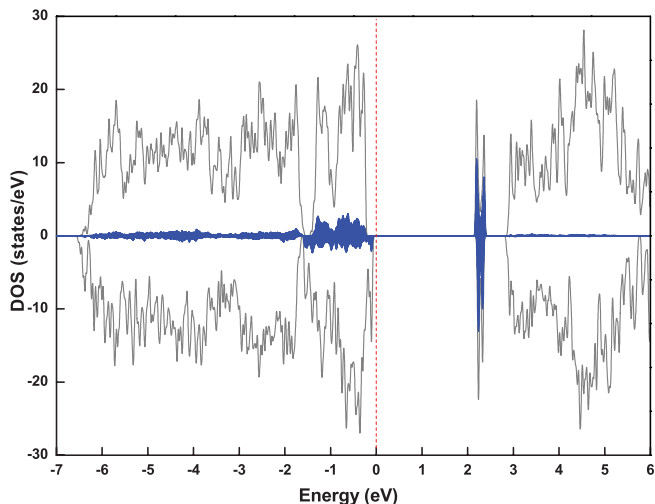


FIG. 7. (Color online) DOS for the  $\text{Co}^{3+}$  impurity in  $\text{Cr}_2\text{O}_3$ .

The  $\text{Ni}^{3+}$  ion is formally  $3d^7$ . Here again, different spin states may be possible. In the high-spin state, five electrons would fill the majority-spin  $3d$  shell, and the remaining two electrons would occupy two of the  $t_{2g}$  states. Calculations show, however, that this state is unstable. In the stable low-spin state, six electrons fill the  $t_{2g}$  levels (as in the Co-doped system), and the remaining one electron occupies one  $e_g$  state. The partial DOS for Ni is shown in Fig. 8. The filled impurity  $t_{2g}$  states for both spin directions lie deep in the valence band, whereas, the Ni  $e_g$  states form impurity levels in the band gap.

Compensation by other defects and co-doping may affect the position of the Fermi level and, thereby, the charge state of the impurities. In particular, there is evidence that Ti mainly substitutes as  $\text{Ti}^{4+}$  compensated by Cr vacancies and associated in complex defects.<sup>24</sup> Such aliovalent substitution is particularly likely if a filled or empty impurity level lies close to the middle of the band gap as in the case of Ti (see Fig. 3). Ni is another such case (Fig. 8) where a low-lying empty level for majority-spin electrons may be filled, producing a

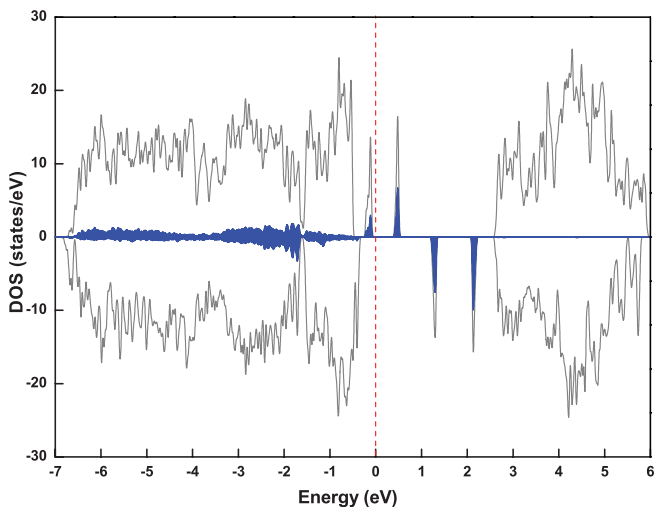


FIG. 8. (Color online) DOS for the  $\text{Ni}^{3+}$  impurity in  $\text{Cr}_2\text{O}_3$ .

negatively charged impurity state corresponding to the  $\text{Ni}^{2+}$  ion. Therefore, in addition to the neutral impurity states described above, we considered the positively charged  $\text{Ti}^{4+}$  and negatively charged  $\text{Ni}^{2+}$  states. These states are modeled by introducing a homogeneous background charge in the calculation before optimizing the atomic structure. The  $\text{Ti}^{4+}$  dopant introduces two  $t_{2g}$ -like impurity levels in both spin channels close to the conduction-band bottom.  $\text{Ni}^{2+}$  has a formal local moment of  $2\mu_B$  with a fully occupied majority-spin  $3d$  shell (including two  $e_g$ -like majority-spin impurity states near the valence-band maximum) and no impurity states in the minority-spin spin channel.

## B. Structural features

As seen in Table I, three dopants (Ti, Mn, and Ni) induce a Jahn-Teller distortion (in these cases, the equivalence of the triples of bonds is broken). Since the true cation site symmetry in  $\text{Cr}_2\text{O}_3$  is not octahedral but  $C_3$ , the  $t_{2g}$  states are slightly split into a lower-lying doublet and a singlet. Thus, in the case of Ti, the Jahn-Teller effect is induced by one  $3d$  electron occupying a doubly degenerate ground state derived from  $t_{2g}$ , but in the case of V, there is no symmetry breaking. For Mn and Ni dopants, the Jahn-Teller distortion is induced by the occupation of one of the two degenerate  $e_g$ -like states, which remain degenerate in the  $C_3$  crystal field.

In order to find the ground-state structure for the Jahn-Teller impurities, we performed a series of calculations with different initial distortions from the symmetric structure. We found two types of distorted structures *A* and *B* shown in Fig. 9. For Ti and Mn impurities, the ground state is the same in the two supercells: structure *A* for Ti and structure *B* for Mn, although the magnitude of the Jahn-Teller distortion is notably different in the two supercells. For the Ni impurity, structure *A* (structure *B*) is the ground state in the mixed (hexagonal) cell. These results indicate that the finite-size effects have a large effect on the Jahn-Teller distortion.

For the Ni impurity, the filled majority-spin  $e_g$  state is separated from the empty one by about 0.5 eV. This splitting is not due to the Hubbard  $U$  interaction. (The Ni  $e_g$  states strongly hybridize with the O  $2p$  states, and as a result, the impurity levels carry the large weight of the O  $2p$  states; this makes the Hubbard  $U$  splitting ineffective.) Instead, this splitting is mainly due to the Jahn-Teller distortion, and, in fact, similar splitting is observed for the empty minority-spin Ni  $e_g$  states. In contrast, in the case of Mn, the splitting between the filled

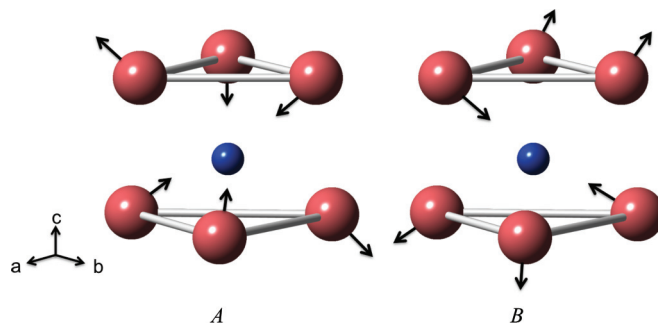


FIG. 9. (Color online) Schematic of two types of distortions found for Jahn-Teller impurities. Left: structure *A*; right: structure *B*.

and the empty majority-spin  $e_g$  states is electronically driven. (In the unrelaxed structure, this splitting is similar.)

The interatomic distances listed in Table I are quite similar for the hexagonal and mixed supercells when no Jahn-Teller distortion is present. The variation in the distances between the impurity and its neighbors (Table I) can be understood as follows. Generally, as the nuclear charge is increased, the spatial extent of the  $3d$  wave function is reduced, and the interatomic distances systematically contract. This general trend is seen in Table I with the notable exceptions of Mn, Fe, and Ni. For each of these dopants, the extra (relative to the preceding element) electron occupies an  $e_g$ -like impurity level; the latter are, in fact, antibonding hybrids of the dopant  $e_g$  and oxygen  $2p$  orbitals. Occupation of these orbitals weakens the bonding with the neighboring oxygen atoms, which, thereby, shift outward. As a result, the general trend of decreasing bond lengths is violated. This explanation is consistent with the fact that the largest bond-length reduction occurs between Fe and Co where two  $e_g$ -like orbitals are depopulated.

The charged states corresponding to the  $Ti^{4+}$  and  $Ni^{2+}$  ions do not have degenerate ground states and are, therefore, not Jahn-Teller active. Indeed, for the  $Ni^{2+}$  ion as well as for  $Ti^{4+}$  in the hexagonal cell, the symmetry of the impurity site is not broken (see Table I). However, in the mixed cell, the  $Ti^{4+}$  ion with an empty  $3d$  shell develops a small displacement from the symmetric position. This distortion is probably caused by the pseudo-Jahn-Teller effect<sup>25</sup> and is driven by the hybridization between Ti and the neighboring oxygens. Due to the fact that the  $3d$  shell of the  $Ti^{4+}$  ion is empty, the displacement can lead to substantial energy gain from this hybridization, which competes with the elastic energy cost. This energy balance is apparently rather delicate since the presence of distortion depends on the choice of the supercell.

### C. Magnetic interaction

To estimate the effect of substitution on the Néel temperature, we have calculated the exchange energies for the impurities as well as for their four Cr neighbors as explained in Sec. II. These exchange energies are listed in Table II for both types of supercells. These values are compared with the exchange energy calculated for the Cr ion in pure  $Cr_2O_3$  evaluated using both supercells. The exchange energy for the host material agreed with the value calculated in Ref. 11 where the exchange parameters were also calculated and the Néel temperature was found to be in good agreement with experiment.<sup>11</sup>

Note that, in the hexagonal supercell, there are only two Cr atoms per buckled honeycomb layer. Substitution of one Cr atom by a dopant, therefore, results in one Cr layer being 50% substituted, and all in-plane neighbors of Cr in that layer are dopants. Therefore, the exchange energy ( $E_2$ ) for the in-plane Cr neighbors of the dopant in the hexagonal cell is not representative of an isolated impurity.

First, we see differences in the exchange energies calculated using two different types of supercells. Since the minimal separation between the dopants is larger in the mixed supercell, the corresponding results are likely to be more accurate. More importantly, none of the transition-metal dopants considered here demonstrate a clear tendency to enhance the exchange

coupling in their vicinity. The case of Fe is marginal, but neutron-diffraction studies of the  $Cr_{2-x}Fe_xO_3$  alloy found that the  $T_N$  decreases under Fe doping.<sup>26</sup> Magnetic properties of the concentrated  $Cr_{2-x}Fe_xO_3$  system were recently studied in Ref. 27.

We also observe that the Jahn-Teller displacement of the Ti, Ni, and Mn ions makes the exchange energies for their three second-nearest neighbors quite different from each other. In particular, one of the second neighbors of Ti develops a very large exchange energy of 186 meV. Clearly, the exchange coupling is very sensitive to bond lengths. Note, however, that the Jahn-Teller distortion, as noted above, depends on the choice of the supercell and is, therefore, not accurately represented in our calculations. Moreover, lattice vibrations often strongly renormalize the degree of this distortion and, thereby, reduce the strength of the exchange coupling around the Jahn-Teller ions.<sup>28</sup>

Since the Co impurity has a zero local moment, the exchange energy for it is undefined. It is somewhat surprising that the exchange energy for its next-nearest Cr neighbor in the hexagonal cell remains quite large (83 meV), even though this Cr atom has only one Cr neighbor in this cell (out of four). We have recalculated this energy with all ions fixed at their bulk  $Cr_2O_3$  positions and found that it is reduced to 40 meV. Thus, the exchange parameters are strongly affected by ionic relaxation around the impurities, which is consistent with the large effect of the Jahn-Teller distortion. A similar reduction in the exchange energy was also found in the unrelaxed state for the second neighbor of the weakly coupled Ni and  $Ni^{2+}$  in the hexagonal cell.

Based on the results in Table II, none of the transition-metal impurities considered here can be expected to increase  $T_N$  in  $Cr_2O_3$ .

### V. NITROGEN IMPURITY

The local DOS on the isovalent impurity  $N^{2-}$  ion (see Fig. 10) shows that the dopant introduces two localized levels in the band gap. Since N has a smaller nuclear charge than O, its  $2p$  states lie higher than O  $2p$ . The N  $2p$  triplet is fully split by the crystal field. The lowest N  $2p$  level lies in the valence band. The two remaining N  $2p$  states fall into the band gap. These gap levels are strongly hybridized with the  $e_g$  states of the neighboring Cr ions.

Table III lists the bond lengths between the N ion and its four Cr neighbors. In bulk  $Cr_2O_3$ , each O atom has two pairs of equivalent bonds with Cr. For the N dopant, however, all four bonds become inequivalent. This structural distortion is a special kind of Jahn-Teller effect facilitated by antiferromagnetic ordering. Its mechanism is as follows. Consider one pair of equivalent bonds of O with Cr neighbors. These two Cr atoms belong to different antiferromagnetic sublattices. Although the crystal field splits the O  $2p$  level in three singlets, spin degeneracy remains. The  $2p$  electron of a certain spin hybridizes differently with two Cr neighbors, whose local moments are antiparallel. The two resulting hybrid levels of opposite spins are degenerate, but they are spatially oriented toward different Cr neighbors. Note that this is not the Kramers degeneracy since time-reversal symmetry is broken. Although in bulk  $Cr_2O_3$  these levels are equally populated,

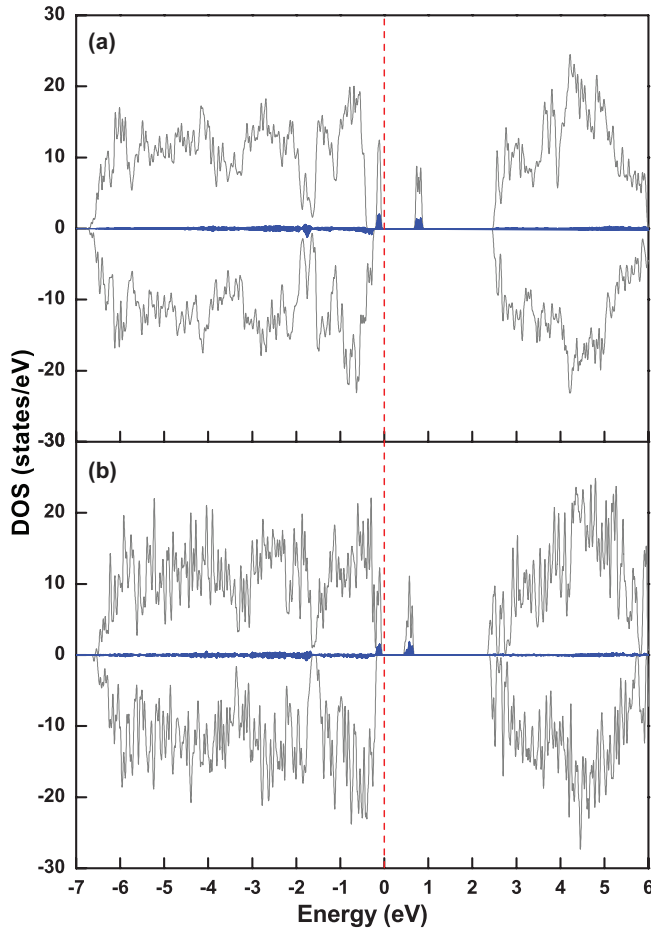


FIG. 10. (Color online) DOS for the  $N^{2-}$  impurity in  $Cr_2O_3$ . (a) With the normal number of electrons (b) in the Slater transition state. The unfilled black line is the total DOS, whereas, the blue shaded area indicates the local DOS on the N impurity.

a charge-neutral N dopant removes one electron, and the structural symmetry is broken. (A similar distortion occurs for the isovalent  $B^{2-}$  dopant.) Note that this type of Jahn-Teller distortion only appears due to the antiferromagnetic order; similar doping of nonmagnetic time-reversal invariant  $Al_2O_3$  with Kramers degeneracy does not break the structural symmetry.<sup>29</sup>

Due to spin-lattice coupling, the equilibrium structures corresponding to different spin configurations are generally different. These lattice relaxations reduce the energy differences between the excited spin states and the ground-state

configuration. Since the transition-metal dopants considered in Sec. IV do not have a positive effect on  $T_N$ , we did not consider the role of spin-lattice coupling for them. As we see below, for N and B dopants, the situation is different. An accurate description of magnetic thermodynamics in the presence of the spin-lattice coupling is a difficult problem. Whether the effective spin Hamiltonian is better represented by unrelaxed or relaxed total energies may depend on the particular system. For example, in the special case when the system is harmonic and the spin-lattice coupling is limited to terms linear in lattice displacements, the phonons can be integrated out to give a constant term, and the exact spin Hamiltonian then contains fully relaxed energies. However, this is no longer true if the system is anharmonic or if the force-constant matrix depends on the spin configuration (which it generally does). One may expect that the unrelaxed and fully relaxed energy differences represent the possible range for the effective spin energies that determine  $T_N$ . Therefore, we consider both cases for N and B impurities.

The exchange energies for the four Cr neighbors of N are given in Table IV. By default, the energy differences are calculated at fixed structures, but fully relaxed energies are included in brackets where available. If we start with the bulk magnetic configuration, the exchange energies for two nearest neighbors of the N impurity (Cr atoms 1 and 2) are negative. This means that the N impurity changes the exchange coupling so strongly that the ground-state configuration becomes different with the spin on Cr atom 1 reversed. If we start from this ground-state configuration, the exchange energies for Cr atoms 1 and 2 are positive and large [see the column N (GS) in Table IV]. This indicates that the exchange coupling between Cr atoms 1 and 2 has been made strongly ferromagnetic by the N impurity. The origin of this coupling is discussed below when we compare the effects of N and B impurities. There is a strong spin-lattice coupling as can be seen from a large reduction in the exchange energies if the structural relaxation is included (see energies in brackets). Strong ferromagnetic coupling between Cr atoms 1 and 2 should negatively affect the exchange energies of their own neighbors and should tend to destabilize the antiferromagnetic order.

The LDA usually places the filled localized Kohn-Sham orbitals too high and empty localized levels too low. In order to determine the positions of the impurity levels in the band gap, a correction may need to be used. For the transition-metal impurities considered above, the localized states in the band gap have a mainly  $3d$  character of the dopant ion; the Hubbard

TABLE III. Bond lengths  $d_i$  (Å) between the anion dopant and its four Cr neighbors. The impurity is isovalent unless the formal ionic charge is specified. For N, both antiferromagnetic (AFM) and ground state (GS, in which one neighboring Cr has a reversed spin) magnetic configurations are included. The labeling of Cr atoms is the same in all cases.

Anion	O	N (AFM)		N (GS)		N <sup>3-</sup>		N <sup>1-</sup>		B		B <sup>3-</sup>		B <sup>1-</sup>	
		Bulk	Hex	Mix	Hex	Mix	Hex	Mix	Hex	Mix	Hex	Mix	Hex	Mix	Hex
$d_1$	1.96	1.98	1.97	1.86	1.86	1.93	1.94	2.08	2.06	1.92	1.90	1.97	1.95	2.02	1.98
$d_2$	1.96	1.80	1.81	1.89	1.88	1.93	1.94	1.68	1.69	2.10	2.09	1.97	1.95	2.02	1.98
$d_3$	2.01	2.11	2.11	2.13	2.13	1.97	1.98	2.13	2.14	2.11	2.08	2.16	2.16	2.20	2.20
$d_4$	2.01	1.99	1.98	1.98	1.98	1.97	1.98	2.04	2.10	2.19	2.24	2.16	2.16	2.20	2.20

TABLE IV. Exchange energies  $E_i$  (meV units) for the four Cr neighbors of the anion in both hexagonal and mixed cells. Numbering of Cr atoms and other notation is the same as in Table III. Values in brackets include lattice relaxation.

Anion Cell	N (AFM)		N (GS)		N <sup>3-</sup>		N <sup>1-</sup>		B		B <sup>3-</sup>		B <sup>1-</sup>	
	Hex	Mix	Hex	Mix	Hex	Mix	Hex	Mix	Hex	Mix	Hex	Mix	Hex	Mix
$E_1$	-76	-111	385 (184)	374 (202)	111	98	48	-13	386 (344)	504 (361)	130 (31)	185 (51)	314	431 (334)
$E_2$	-6	11	597 (427)	577 (388)	111	98	14	-42	195 (108)	323 (242)	130 (31)	185 (51)	314	431 (334)
$E_3$	146	166	147 (131)	170 (159)	129	107	59	84	387 (320)	422 (352)	457 (276)	473 (230)	288	290 (216)
$E_4$	242	231	158 (70)	247 (145)	129	107	240	189	332 (251)	276 (224)	457 (276)	473 (230)	288	290 (216)

$U$  interaction, to a large extent, corrects for the self-interaction in those cases. However, for anion dopants, the impurity states are strongly delocalized to several surrounding Cr atoms, and the Hubbard  $U$  correction is unable to capture the discontinuity of the exchange-correlation potential between the filled and the empty states. The positions of the impurity levels may have a significant effect on the exchange interaction.<sup>30</sup> Of particular importance are shallow impurity states since they extend over several neighbors and can effectively mediate the exchange interaction. The correct position of the highest occupied level corresponds to the electron removal energy, which can be approximately found using the Slater transition state (STS) method.<sup>31</sup> In this method, the eigenvalue corresponding to the highest occupied level is evaluated for the STS in which the occupation of that level is reduced from 1 to 1/2.

Figure 10(b) shows the DOS for the N impurity calculated for the STS (with the ionic configuration obtained for the neutral system). It is seen that the shallow impurity state moves toward the valence band in the STS, indicating that the LDA potential places it too high. In order to assess the effect of this shift on the exchange interaction, we have recalculated the exchange energies using the local force theorem applied with respect to the STS. In other words, for each magnetic configuration, we took the self-consistent total energy of the STS and added the single-particle energy difference between the system with the correct electron count and the STS. This procedure is approximate because STS does not provide a more accurate electronic structure than the neutral system. However, by evaluating the exchange energies using the STS potential, we can assess the error associated with misplacing the highest occupied impurity level and, thereby, inaccurately representing its wave function. We have found that the exchange energies evaluated in this way are close to the straightforward total energy calculation (for example,  $E_i = -108, 16, 164,$  and  $245$  meV for the mixed supercell).

Due to the presence of a low-lying empty impurity level (Fig. 10), the N ion may be easily converted to the charged N<sup>3-</sup> state. On the other hand, co-doping with Mg was shown to turn Cr<sub>2</sub>O<sub>3</sub> into a  $p$ -type conductor<sup>32</sup> where nitrogen should be in the N<sup>1-</sup> state. We have considered both of these charged impurity states by introducing a homogeneous background charge. For the N<sup>3-</sup> state, the structural and magnetic symmetries are restored (Table III), and two impurity levels in each spin channel lie within 1 eV from the valence-band maximum (DOS not shown). However, for the N<sup>1-</sup> state, the structure is strongly distorted (Table III), and the two empty impurity states of the same spin again lie within 1 eV of the valence-band maximum. (Several empty impurity states also

split off from the conduction band in this state.) We were also able to converge a structurally symmetric state with a zero total magnetic moment for the N<sup>1-</sup> impurity, but its total energy lies  $\sim 0.14$  eV higher compared to the distorted state with the total moment of  $2\mu_B$ .

The exchange energies for charged N-doped systems are shown in Table IV. For the N<sup>1-</sup> ion, the reversal of the local moment on the nearest-neighbor Cr ion also reverses the spin of the impurity levels, which is included in  $E_1$ . Without attempting to uncouple these spins, one can argue that the impurity spins are strongly coupled to the nearest-neighbor Cr and behave as a rigid complex with it. In this approximation, the value of  $E_1$  correctly represents the effective spin interactions. It is clear that N<sup>1-</sup> dopants should reduce  $T_N$ . On the other hand, the exchange energies near the N<sup>3-</sup> impurities are almost unchanged compared to bulk Cr<sub>2</sub>O<sub>3</sub>.

## VI. BORON IMPURITY

Figure 11(a) shows the total DOS for the case of a boron impurity in the hexagonal supercell along with the partial DOS on the B atom. (In the mixed cell, the shallow filled impurity levels are slightly spin split, but otherwise, the DOS is similar; see Supplemental Material.<sup>22</sup>) The impurity introduces three localized levels in the band gap. These levels originate from the B  $2p$  states that are split by the crystal field. Due to its smaller nuclear charge, B  $2p$  levels are pushed to even higher energies than those of N so that all of them fall in the gap. Note, however, that the impurity states have a large admixture of the  $3d$  (mainly  $e_g$ ) states on the nearby Cr atoms. This is clearly seen in Fig. 12, which shows the local DOS on the Cr neighbors of the B atom and from the charge density of the impurity states. In particular, Fig. 13 shows the charge density for the shallow occupied impurity level, which is clearly a hybrid state extending between B and its Cr neighbors.

The exchange energies for the four Cr neighbors of the impurity B ion are listed in Table IV. As for the case of N, the relaxed energies are included in brackets where available. The exchange energies are strongly enhanced compared to bulk Cr<sub>2</sub>O<sub>3</sub>, even if relaxation is included. This enhancement is due to the impurity states mediating strong hybridization between the nearby Cr ions, which depends on the mutual orientation of the Cr spins.

Comparing the N and B impurities, we see that N frustrates the AFM order around it, whereas, B reinforces it. To understand this difference, we need to focus on the interaction between the localized impurity states and the

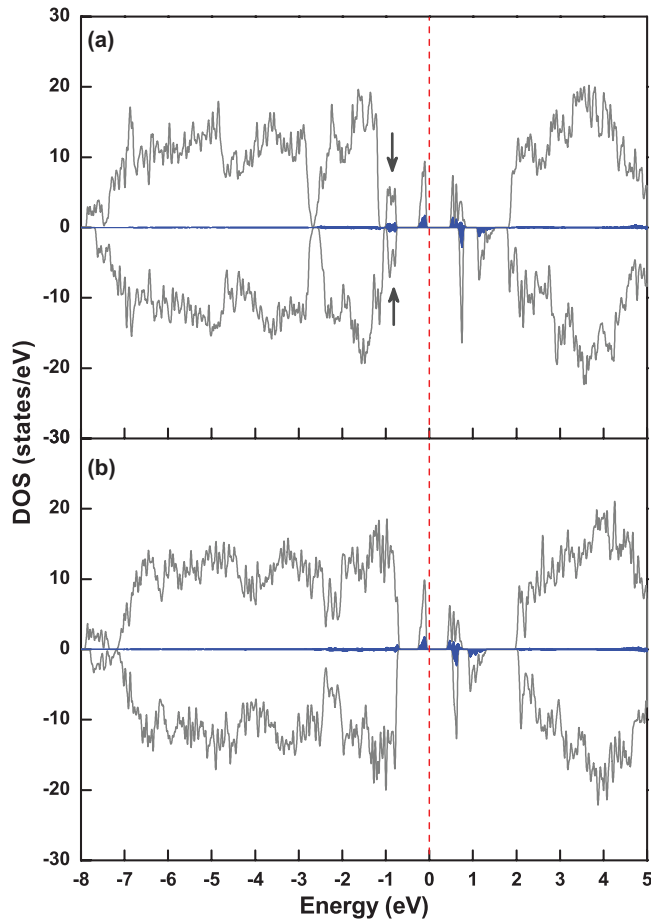


FIG. 11. (Color online) DOS for B impurity in  $\text{Cr}_2\text{O}_3$ . (a) With the normal number of electrons (b) in the Slater transition state. The unfilled black line is the total DOS, whereas, the blue shaded area indicates the local DOS on the B impurity.

magnetic moments of the nearby Cr atoms. For each impurity state, on-site Hund exchange favors parallel alignment of its spin with those of the Cr atoms participating in its formation, generating ferromagnetic coupling between them. A similar mechanism can produce bound magnetic polarons in dilute ferromagnetic oxides (see, e.g., Ref. 33 and references therein). In our present case, this interaction is superimposed on the existing AFM order, and the magnetic ground state is determined by the best compromise between the two generally competing mechanisms. In the N-doped system, the magnetic polaron mechanism wins over, and the magnetic ground state is obtained by aligning three of the four nearby Cr spins parallel to each other with the single filled impurity state almost fully localized on them (see Fig. 8 in the Supplemental Material<sup>22</sup>). In the B-doped system, there are two additional shallow states in the opposite spin channels [arrows in Fig. 11(b) and charge density in Fig. 13], but these states are localized on different pairs of Cr atoms. Thanks to the favorable hybridization geometry, in the AFM ground state, the Hund exchange with these states is fully saturated for all four Cr neighbors (see Fig. 13). Note that the spins on Cr sites 1 and 3 are down and those on sites 2 and 4 are up, all parallel to the spins of the localized states extending to these sites. Therefore, ferromagnetic coupling, induced by the shallow

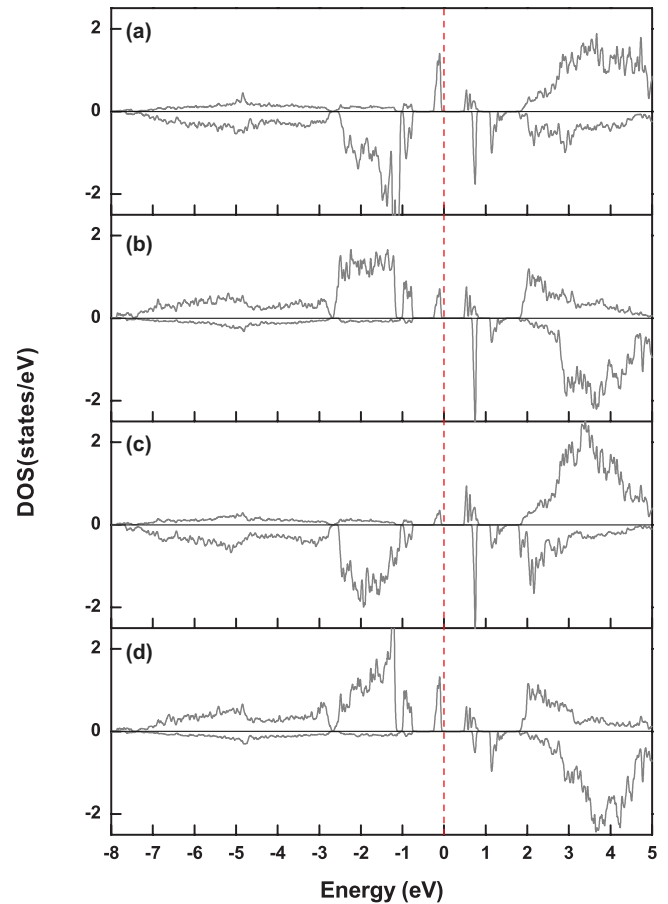


FIG. 12. (Color online) Partial DOS on the Cr neighbors of the B impurity. Panels (a)–(d) correspond to the Cr atoms in the order of Table III.

localized states, reinforces the AFM order and results in an overall enhancement of the exchange energies. According to this picture, filling of the second deep impurity level in the B-doped system, which is formed by Cr ions with opposite spins (see Fig. 12), should reduce the exchange energies. This reduction is indeed observed for the  $\text{B}^{3-}$  case, particularly, if the relaxations are taken into account (see Table IV).

As discussed above for the N dopant, the position of the highest occupied impurity level can be found more accurately from the DOS in the STS, which is shown in Fig. 11(b). It is, however, seen that the corrected impurity level shifts only slightly to lower energies. We have also checked that

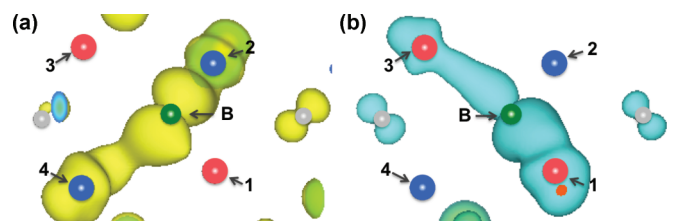


FIG. 13. (Color online) Isosurfaces of the charge density ( $0.034 e/\text{\AA}^3$ ) for the shallow impurity states shown by arrows in Fig. 11(a). (a) Majority spin; (b) minority spin. Cr atoms are labeled as in Table III. Unmarked gray spheres show O ions.

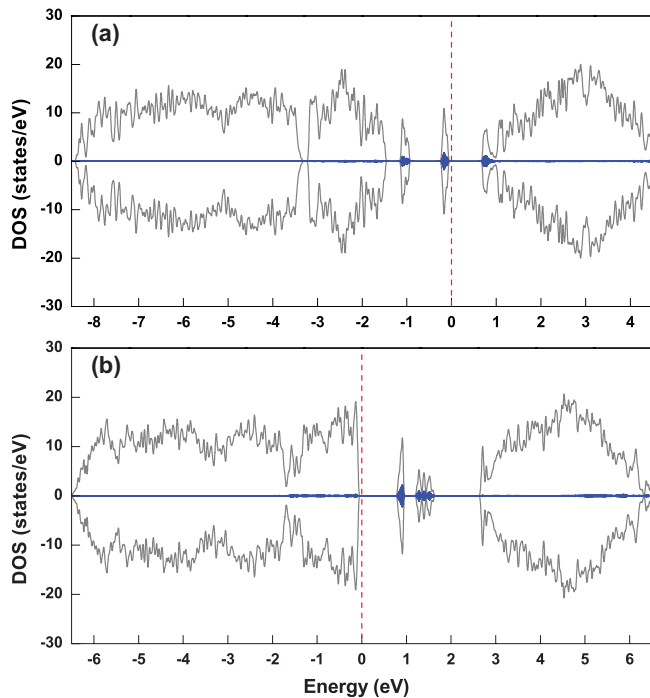


FIG. 14. (Color online) DOS for the charged B impurities in  $\text{Cr}_2\text{O}_3$ . (a)  $\text{B}^{3-}$  state. (b)  $\text{B}^{1-}$  state. Solid line: total DOS; blue shaded area: partial DOS on B.

the exchange energies calculated using the STS potential (as explained above for N) are very close to the values listed in Table IV.

We have seen above that the supercells used here are not large enough to accurately determine the amount of the Jahn-Teller distortion in Ti-, Mn-, and Ni-doped  $\text{Cr}_2\text{O}_3$ . The boron-doped system is similar in this respect as seen from Tables III and IV. In particular, the exchange energy for the nearest Cr neighbor of B is much larger in the mixed supercell compared to the hexagonal one. This difference, however, does not affect the overall conclusions since the average enhancement of the exchange energies around the B dopant is very high in supercells of both kinds.

We also considered aliovalent  $\text{B}^{3-}$  and  $\text{B}^{1-}$  impurity states by introducing a homogeneous background charge. The DOS for these two cases are shown in Fig. 14. As explained above, in these states, the electron count is even, and there is no Jahn-Teller distortion; full spin symmetry is, therefore, seen in the DOS plots. As expected, the addition (or removal) of an electron not only changes the occupations of the impurity states, but also shifts their positions up (or down). In the  $\text{B}^{1-}$  charge state, the low-lying levels merge with the valence band.

The exchange energies for the charged systems are listed in Table IV. Due to the restoration of the structural symmetry, the effect of acceptor and donor co-doping is not uniform on the

different Cr neighbors of B. For  $\text{B}^{1-}$ , the exchange energies remain large, particularly, if the relaxations are not included. However, as noted above, for the  $\text{B}^{3-}$  charge state, the relaxed exchange energies for the two nearest Cr neighbors are reduced compared to bulk  $\text{Cr}_2\text{O}_3$ . Strong spin-lattice coupling does not allow us to draw a definite conclusion about the effect of  $\text{B}^{3-}$  impurities on  $T_N$ , but it is clear that this charge state is, at any rate, less favorable than  $\text{B}^{2-}$  or  $\text{B}^{1-}$ .

The motivation for increasing  $T_N$  of  $\text{Cr}_2\text{O}_3$  is due to its applications in magnetoelectric devices. For these applications, it is important that  $\text{Cr}_2\text{O}_3$  retains its room-temperature insulating properties under doping. Therefore, we should insist that the dopants do not introduce shallow donor or acceptor states. Inspecting the DOS of the three charge states considered here, we see that the neutral state retains a large excitation gap of about 2 eV for both valence and conduction bands (i.e., for the transitions from the valence band to the lowest unoccupied impurity state and from the highest occupied impurity state to the conduction band). For both  $\text{B}^{3-}$  and  $\text{B}^{1-}$  charged states, the excitation gap is reduced to about 1 eV (Fig. 14). Therefore, the neutral state is preferable for magnetoelectric applications.

To estimate the enhancement of  $T_N$  under boron doping, we take into account that each B atom substituted for O (in the 2- or 1- charge state) enhances the exchange energy on its four Cr neighbors by a factor of 2 to 3 (see Table IV). This means that  $T_N$  should grow at the rate of 5%–10% per 1% of boron substitution. This enhancement is sufficiently large to be attractive for practical purposes.

## VII. CONCLUSIONS

We have used electronic structure calculations to explore the possibility of enhancing the Néel temperature  $T_N$  of  $\text{Cr}_2\text{O}_3$  by substitutional doping. We have characterized the electronic structure of substitutional transition-metal dopants as well as that of N- and B-anion dopants. We found that, although transition-metal impurities are detrimental to  $T_N$ , anion doping with B is favorable, at least, as long as the Fermi level lies sufficiently low to avoid substitution in the  $\text{B}^{3-}$  charge state. Boron doping introduces hybrid impurity states, which strongly enhance the exchange energies at the neighboring Cr ions. A rough estimate suggests that 1% B substitution can increase  $T_N$  by 5%–10%. The neutral  $\text{B}^{2-}$  state is favorable for the preservation of the insulating properties of  $\text{Cr}_2\text{O}_3$ .

## ACKNOWLEDGMENTS

This work was supported by the NSF and the Semiconductor Research Corporation through a supplement to the Nebraska MRSEC (Grant No. DMR-0820521). K.D.B. acknowledges financial support from the Research Corporation through a Cottrell Scholar Award.

\*belashchenko@unl.edu

<sup>1</sup>L. D. Landau and E. M. Lifshitz, *Electrodynamics of Continuous Media* (Pergamon, Oxford, 1960).

<sup>2</sup>M. Fiebig, *J. Phys. D* **38**, R123 (2005).

<sup>3</sup>P. Borisov, A. Hochstrat, X. Chen, W. Kleemann, and C. Binck, *Phys. Rev. Lett.* **94**, 117203 (2005).

- <sup>4</sup>C. Binek and B. Doucin, *J. Phys.: Condens. Matter* **17**, L39 (2005).
- <sup>5</sup>Xi He *et al.*, *Nat. Mater.* **9**, 579 (2010).
- <sup>6</sup>N. A. Spaldin and M. Fiebig, *Science* **309**, 391 (2005).
- <sup>7</sup>W. Eerenstein, N. D. Mathur, and J. F. Scott, *Nature (London)* **442**, 759 (2006).
- <sup>8</sup>R. Ramesh and N. A. Spaldin, *Nat. Mater.* **6**, 21 (2007).
- <sup>9</sup>H. Bea, M. Gajek, M. Bibes, and A. Barthelemy, *J. Phys.: Condens. Matter* **20**, 434221 (2008).
- <sup>10</sup>M. Bibes and A. Barthélémy, *Nat. Mater.* **7**, 425 (2008).
- <sup>11</sup>S.-Q. Shi, A. L. Wysocki, and K. D. Belashchenko, *Phys. Rev. B* **79**, 104404 (2009).
- <sup>12</sup>K. Sato *et al.*, *Rev. Mod. Phys.* **82**, 1633 (2010).
- <sup>13</sup>A. I. Liechtenstein, V. I. Anisimov, and J. Zaanen, *Phys. Rev. B* **52**, R5467 (1995).
- <sup>14</sup>J. Velev, A. Bandyopadhyay, W. H. Butler, and S. Sarker, *Phys. Rev. B* **71**, 205208 (2005).
- <sup>15</sup>P. E. Blöchl, *Phys. Rev. B* **50**, 17953 (1994).
- <sup>16</sup>G. Kresse and J. Hafner, *Phys. Rev. B* **48**, 13115 (1993).
- <sup>17</sup>G. Kresse and J. Furthmüller, *Phys. Rev. B* **54**, 11169 (1996).
- <sup>18</sup>H. Monkhorst and J. D. Pack, *Phys. Rev. B* **13**, 5188 (1976).
- <sup>19</sup>A. Rohrbach, J. Hafner, and G. Kresse, *Phys. Rev. B* **70**, 125426 (2004).
- <sup>20</sup>N. J. Mosey, P. Liao, and E. A. Carter, *J. Chem. Phys.* **129**, 014103 (2008).
- <sup>21</sup>E. J. Samuelsen, M. T. Hutchings, and G. Shirane, *Physica* **48**, 13 (1970).
- <sup>22</sup>See Supplemental Material at <http://link.aps.org/supplemental/10.1103/PhysRevB.87.054435> for the DOS of the mixed supercell.
- <sup>23</sup>A. B. Shick, W. E. Pickett, and A. I. Liechtenstein, *J. Electron Spectrosc. Relat. Phenom.* **114–116**, 753 (2001).
- <sup>24</sup>A. Atkinson, M. R. Levy, S. Roche, and R. A. Rudkin, *Solid State Ionics* **177**, 1767 (2006).
- <sup>25</sup>I. B. Bersuker, *The Jahn-Teller Effect* (Cambridge University Press, Cambridge UK, 2006).
- <sup>26</sup>D. E. Cox, W. K. Takei, and G. Shirane, *J. Phys. Chem. Solids* **24**, 405 (1963).
- <sup>27</sup>H. Sadat Nabi and R. Pentcheva, *Phys. Rev. B* **83**, 214424 (2011).
- <sup>28</sup>K. I. Kugel and D. I. Khomskii, *Sov. Phys. Usp.* **25**, 231 (1982).
- <sup>29</sup>A. Stashans, E. Kotomin, and J.-L. Calais, *Phys. Rev. B* **49**, 14854 (1994).
- <sup>30</sup>A. Zunger, S. Lany, and H. Raebiger, *Phys.* **3**, 53 (2010).
- <sup>31</sup>J. C. Slater, *The Self-Consistent Field Theory for Molecules and Solids: Quantum Theory of Molecules and Solids*, Vol. 4 (McGraw-Hill, New York, 1974).
- <sup>32</sup>E. Arca, K. Fleischer, and I. V. Shvets, *Appl. Phys. Lett.* **99**, 111910 (2011).
- <sup>33</sup>J. M. D. Coey, M. Venkatesan, and C. B. Fitzgerald, *Nat. Mater.* **4**, 173 (2005).